Opto-Electronic Advances

Review

2018, Vol. 1, No. 9

DOI: 10.29026/oea.2018.180015

Sensing and lasing applications of whispering gallery mode microresonators

Yu Zheng[1,2], Zhifang Wu[2,3]*, Perry Ping Shum[1,2]*, Zhilin Xu[4], Gerd Keiser[5], Georges Humbert[6], Hailiang Zhang[1,2], Shuwen Zeng[6] and Xuan Quyen Dinh[2,7]

Optical whispering gallery mode (WGM) microresonators have attracted great attention due to their remarkable properties such as extremely high quality factor, small mode volume, tight confinement of modes, and strong evanescent field. All these properties of WGM microresonators have ensured their great potentials for applications, such as physical sensors, bio/chemical sensors and microlasers. In this mini-review, the key parameters and coupling conditions of WGM microresonators are firstly introduced. The geometries of WGM optical microcavities are presented based on their fabrication methods. This is followed by the discussion on the state-of-the-art applications of WGM microresonators in sensors and microlasers.

Keywords: WGM microresonators; sensors; microlasers; microcavities

Zheng Y, Wu Z F, Shum P P, Xu Z L, Keiser G *et al*. Sensing and lasing applications of whispering gallery mode microresonators. *Opto-Electronic Advances* **1**, 180015 (2018).

Introduction

The whispering gallery mode (WGM) was first discovered by Lord Rayleigh in sound waves in 1910, when he studied the phenomenon of whispering gallery in St Paul's Cathedral[1]. Then, in 1961 Garrett et al. found that optical waves, which can undergo reflection, refraction and diffraction like a sound waves, can generate WGM in an optical resonator as well[2]. In WGM optical resonators, light with specific wavelengths is confined near a circular ring boundary via total internal reflection.

WGM microresonators have been extensively studied since they allow ultrahigh quality factor (Q factor), small mode volume, and a strong evanescent field. These remarkable properties have led to myriads of applications in extremely sensitive sensors. For example, the sensitivity of bio/chemical sensors based on WGM microresonators is as high as single atomic ions level[3–5]. Moreover, due to extraordinarily high Q factor and small mode volume, WGM microresonators have another important application in microlasers. The WGM-based microlasers own some excellent properties and advantages such as ultralow lasing threshold[6] and extremely narrow linewidth[7]. For instance, the pump threshold of an optofluidic microlaser based on WGM resonance could be down to 0.1 μJ/mm^2 [8]. Compared with many good reviews on WGM[6,9–12], in this paper we will emphasize the current state of the art of WGM sensors and mcirolasers, especially in terms of the sensing sensitivity and the pump threshold respectively. In this paper, the key parameters and coupling conditions of WGM microresonators are discussed first. Then, we present some common geometries based on their fabrication processes. Finally, we focus on the recent progresses on applications of WGM microresonators in sensing and lasing fields.

[1]COFT, School of EEE, Nanyang Technological University, Singapore 639798, Singapore; [2]CINTRA, CNRS/NTU/Thales Research Alliance, Singapore 637553, Singapore; [3]Fujian Key Laboratory of Light Propagation and Transformation, College of Information Science and Engineering, Huaqiao University, Xiamen 361021, China; [4]Center for Gravitational Experiments, School of Physics, Huazhong University of Science and Technology, Wuhan 430074, China; [5]Department of Electrical and Computer Engineering, Boston University, Boston 02215, USA; [6]XLIM Research Institute, UMR 7252 CNRS/University of Limoges, Limoges 87060, France; [7]R&T, Thales Solutions Asia Pte Ltd, Singapore 498755, Singapore

* Correspondence: Z F Wu, E-mail: wzh.fang@gmail.com; P P Shum, E-mail: epshum@ntu.edu.sg

Received 27 August 2018; accepted 25 October 2018; accepted article preview online 1 November 2018

Key parameters and coupling conditions of WGM microresonators

Resonant wavelength

For preliminarily understanding how WGMs are formed in the microcavities, we can consider WGMs in a 2D model, as shown in Fig. 1. Supposing the system is lossless, the constructive interference will occur among the propagating light waves when the total propagation distance is equal to integer multiples of the resonant wavelength. These wavelengths will satisfy the following equation[13]:

$$m\lambda = 2\pi R n_{\text{eff}} \quad , \tag{1}$$

where m, an integer number, is the azimuthal mode number, λ is the resonant wavelength, R is the radius of the microcavity, and n_{eff} is the effective refractive index of the microcavity.

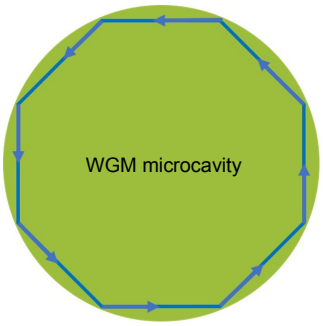

Fig. 1 | Schematic of light trapping inside a WGM microcavity by frustrated total internal reflection.

WGM microcavities can propagate simultaneously transverse magnetic (TM) modes and transverse electric (TE) modes. A numerical approximation of WGM resonances was developed by Lam et al. in 1992[14]. The more accurate resonant wavelengths are expressed as[15]:

$$\lambda^{-1}(R,n_1,n_r,r,m) = \frac{1}{2\pi R n_1}\left[m+\frac{1}{2}+2^{-\frac{1}{3}}\eta(r)\left(m+\frac{1}{2}\right)^{\frac{1}{3}} - \frac{L}{(n_r^2-1)^{\frac{1}{2}}} + \frac{3}{10}\cdot 2^{\frac{2}{3}}\cdot\eta^2(r)\left(m+\frac{1}{2}\right)^{-\frac{1}{3}} - 2^{-\frac{1}{3}}\left(n_r^2-\frac{2}{3}L^2\right)\frac{\eta(r)\left(m+\frac{1}{2}\right)^{-\frac{2}{3}}}{(n_r^2-1)^{\frac{3}{2}}}\right] , \tag{2}$$

where r is the radial mode number, $n_r=n_1/n_2$, n_1 and n_2 are the refractive indices of microcavity and ambient materials, respectively, $\eta(r)$ is the Airy function solution and equals 2.338 if r=1, L is the polarization characteristic coefficient and $L=1/n_r$ for TM modes and $L=n_r$ for TE modes.

Quality factor

WGM microcavities with different geometries can obtain significantly high Q factors. To the best of our knowledge, the maximal Q factor has exceeded 10^{11} achieved with fluoride crystalline materials[16]. The Q factor is defined by the resonator's capability to store energy at a specific frequency, and can be measured in the frequency or time domain, as shown in Equation (3).

$$Q_0 = \omega\frac{E_{\text{stored}}}{P_{\text{diss}}} = \omega\tau = \frac{\omega}{\Delta\omega} \quad , \tag{3}$$

where Q_0 is the resonator's intrinsic Q factor, ω is the resonance frequency, E_{stored} is the energy stored in the resonator, P_{diss} is the power dissipated from the resonator, τ is the photon life time (or cavity ring-down time), and $\Delta\omega$ is the resonance linewidth as measured from the frequency spectrum. Theoretically, the intrinsic Q factor of an independent WGM microcavity is determined by several loss factors as expressed by[17]:

$$Q_0^{-1} = Q_{\text{mat}}^{-1} + Q_{\text{rad}}^{-1} + Q_{\text{sca}}^{-1} + Q_{\text{cont}}^{-1} \quad , \tag{4}$$

where Q_{mat} is the material loss factor, Q_{rad} is the radiative loss factor, Q_{sca} is the scattering loss factor and Q_{cont} is the contaminant loss factor.

Generally, Q_{mat} caused by material absorption and Rayleigh scattering, is dominant among these loss factors. Q_{mat} can be calculated as:

$$Q_{\text{mat}} = \frac{2\pi n}{\alpha\lambda} \quad , \tag{5}$$

where α is the linear absorption coefficient, n is the refractive index of the microcavity material.

Q_{rad}, the radiative loss factor, is inevitable for all circular geometries and is determined by the curvature of the microcavity boundary. Generally, Q_{rad} can be defined as the ratio between the real and imaginary parts of the wave number. When the angular mode number $l = m$, Q_{rad} can be calculated approximately as follows[18]:

$$Q_{\text{rad}} = \frac{1}{2}\left(m+\frac{1}{2}\right)n^{(2p-1)}(n^2-1)^{\frac{1}{2}}\mathrm{e}^{2T_{r,m}} \quad , \tag{6}$$

where $p = \begin{cases} 0, & \text{for TE polarization} \\ 1, & \text{for TM polarization} \end{cases}$,

$$T_{r,m} = \left(m+\frac{1}{2}\right)(\beta_{r,m} - \tanh\beta_{r,m}) \quad , \tag{7}$$

$$\beta_{r,m} = \cosh^{-1}\left\{ n\left[1-\left(\frac{1}{m+\frac{1}{2}}\right)\left(A_r\left(\frac{2m+1}{4}\right)^{\frac{1}{3}} + \frac{n^{1-2p}}{(n^2-1)^{\frac{1}{2}}}\right)\right]^{-1}\right\} ,$$

where A_r are the roots of the Airy function.

Hence, it is found that Q_{rad} depends on the azimuthal mode number m and radial mode number r, and high order modes lead to lower Q_{rad}[9].

The influence on the Q factor from scattering is mainly due to the surface roughness. It can be expressed as:

$$Q_{\rm sca}=\frac{\lambda^2 R}{\pi^2\sigma_{\rm rms}^2 B}\ , \tag{8}$$

where $\sigma_{\rm rms}$ is the root-mean-squared size and B is the correlation length of roughness. From this equation, it is clear to see that $Q_{\rm sca}$ is proportional to the cavity radius R under the same surface inhomogeneities, which indicates that bigger microcavities can confine light better than smaller ones. Meanwhile, by optimizing the size and length of inhomogeneity, the scattering loss can be reduced.

$Q_{\rm cont}$ defines the influence from the surface contaminants, such as water molecules from the atmosphere. The contaminants can form nanolayers or nanoclusters on the microcavity surface and cause additional absorption and scattering loss.

Mode volume

Another prominent advantage of WGM microcavities as mentioned in the introduction section is the small mode volume. The mode volume can be described as the electromagnetic field localization in a WGM microcavity, and it is an especially important parameter for nonlinear applications. The mode volume of a spherical WGM resonator can be calculated using Equations (9):

$$V=3.4\pi^{\frac{3}{2}}\left(\frac{\lambda}{2\pi n}\right)^3 m^{\frac{11}{6}}\sqrt{m-\nu+1}\ , \tag{9}$$

where λ is the wavelength of the pumping light and ν is the magnetic number.

Optical coupling approaches

Optical WGMs can be excited by using a free-space setup, which is composed of a microcavity and a coupling component. The geometries of such optical microcavities include microspheres[19,20], microrings[21], microdisks[4,22], microbubbles[23–25] and microcapillaries[26,27]. The coupling component, like a prism, an angle-polished fiber, or a tapered fiber, is positioned close to the WGM microcavity, as shown in Fig. 2. The prism coupler is considered as one of the oldest optical couplers[28]. It is suitable for coupling evanescent waves into large-size WGM cavities by frustrated total internal reflection, typically in the diameter range of 1–2 cm[29]. The phase-matching condition and critical coupling can be adjusted by respectively changing the incident angle, and the gap between resonator and prism. To the best of our knowledge, the highest coupling efficiency of a prism coupler was reported around 80%[30]. The angle-polished fiber coupler was first proposed and demonstrated by Ichenko in 1999[31]. The mechanism of such a coupler is basically the same as that of the prism coupler. An angle-polished fiber was shown to provide significant improvement on mode quality over the prism by confining the input beam within its core. However, the output beam of both angle-polished fiber and prism couplers still has to be collected in free space. This limits their applications for compact and integrated devices for in situ measurements. Comparatively, a tapered fiber is more commonly used, because the light is coupled and decoupled in-line within a same fiber. In order to increase the overlap of the evanescent fields between the fiber guided mode and the WGM, the diameter of the tapered fiber is usually less than 2 μm.

Phase matching

Phase matching is one of the critical conditions to obtain high efficiency for light power coupling from one device to another. For WGM coupling, phase matching means that the propagation constant of the proper mode in the coupler is equal to the propagation constant of the WGM in the microcavity. Considering the coupling between a tapered optical fiber and a microsphere as an example, when $l = m$ is assumed, the propagation constant $\beta_{\rm ms}$ of a microsphere can be expressed as[32]:

$$\beta_{\rm ms}=kl/x_{rlm}\ , \tag{10}$$

where k is the free space propagation constant and x_{rlm} is the size parameter that corresponds to the r, l, and m resonance. For the tapered fiber, the fundamental mode will significantly extend out into surroundings, and its propagation constant can be calculated as:

$$\beta_{\rm ft}=\left(k^2n'^2-2.405^2\cdot\left(\frac{\rho}{2}\right)^{-2}\right)^{\frac{1}{2}}\ , \tag{11}$$

where n' is the refractive index of the fiber and ρ is the diameter of the fiber taper. When $\beta_{\rm ms}$=$\beta_{\rm ft}$, the phase matching between the tapered fiber and the microsphere

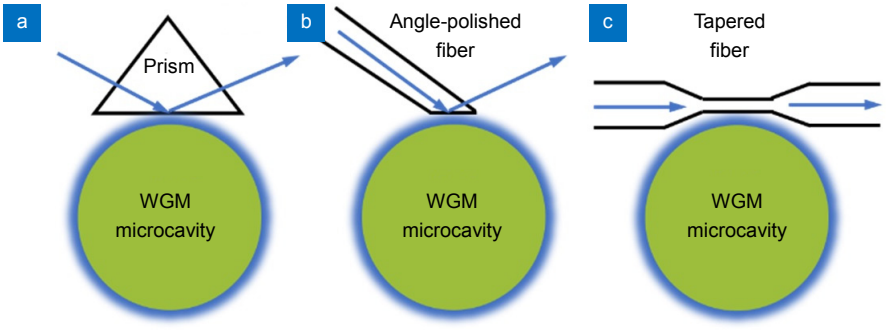

Fig. 2 | Different methods of exciting WGMs. (a) Prism coupling. (b) Polished fiber coupling. (c) Tapered fiber coupling.

is obtained.

Critical coupling

For achieving optimal coupling, besides the satisfaction of phase matching, the distance between the WGM microcavity and the coupler should be properly adjusted in order to exactly compensate the microcavity loss by the amount of power delivered from the coupler. At this time, the coupler output hits zero at the resonant wavelength and the so-called 'critical coupling' is achieved. After the light propagating in the waveguide is coupled into a WGM microcavity with a photon lifetime τ_e, it will resonate along the circular ring boundary and experience intrinsic losses from the microcavity with an intrinsic photon lifetime τ_0[33]. Based on the variation of τ_0 and τ_e, the different coupling regimes can be described as:

1) Undercoupled, $\tau_0<\tau_e$, the cavity intrinsic loss is higher than the input power.

2) Critical coupling, $\tau_0=\tau_e$, the cavity intrinsic loss is equal to the input power.

3) Overcoupled, $\tau_0>\tau_e$, the cavity intrinsic loss is lower than the input power.

Geometries of WGM optical microcavities

Up to now, various geometries, including microspheres, microrings, microdisks, microtoroids, microbottles, microbubbles, and microcapillaries etc. have been demonstrated for exciting WGM. These geometries of microcavities are fabricated from the different materials and methodologies. In this section, these geometries are classified and presented based on their fabrication methods.

Microspheres

Microspheres were the most common microresonator used to generate WGMs in early studies. There are mainly two methods for the fabrication of microspheres, melting of glass materials and the sol-gel process. The former method can be used for a large range of glass materials, since its general principle is to melt the glass materials, which is able to fabricate self-assembly microspheres due to surface tension. One representative method is called fiber splicing. The fiber is first tapered into a proper diameter and then put into one of the arms of the splicer. The fiber tip is melted by the electric arcs and the spherical microcavity is produced by surface tension. By adjusting the power and discharge times of electric arcs generated by the splicer, the diameter of the microsphere can be controlled. The sol-gel process is a chemical synthesis method used to generate microspheres from the molecular level, which is relatively flexible and cheap. The fabrication of silica microspheres based on sol-gel process with the diameter from 150 nm to 2 μm has become a very mature method[12].

Microrings, mirodisks and microtoroids

Due to possessing planar structures, microrings, microdisks and microtoroids are more suitable for photonic integration compared with microspheres. Meanwhile, the fabrication of these planar structures is more controllable. The fabrication methods generally include top-down and bottom-up approaches. Simply, the former one means a small device is produced by removing the useless parts from larger material and adding the other useful parts. The main techniques consist of electron-beam lithography, dry etching and wet chemical etching. For example, Duan et al. reported a simple and robust method to produce well-controlled and uniform $MAPbBr_3$ perovskite-based mircodisk arrays by controlling the concentration of the perovskite precursor, pattern sizes, and hydrophilicity of the substrate[34]. The bottom-up approach normally refers to producing a larger device from smaller materials, such as individual molecules.

Microbottles and microbubbles

The fabrication method of microbottles and microbubbles are similar and more flexible than the first two kinds of geometries[25,38,39]. A simple process of fabricating a microbottle is to taper the optical fiber two times in two adjacent places. Compared with the tubular microcavities, the microbottles have the better ability of light confinement along the cylinder axis. In the early studies, microbubbles were updated from heating microcapillaries with a gas pressure. Recently, some novel methods are applied to fabricate microbubbles[38–40]. For instance, Wang et al. prepared microbubbles based on the drying process of the colloidal quantum dots (CQDs)/polymethyl methacrylate (PMMA) nanocomposite droplets[25].

Applications

Sensors

Generally, the operational mechanism of sensors based on WGM microresonators is to monitor variations of WGM resonance wavelengths induced by physical changes of the system, and the ultrahigh Q factor and the strong evanescent waves make the variations of WGM resonances very sensitive to the surroundings. Hence, WGM microresonators have been developed as a variety of highly sensitive sensors[4,19–21,40], such as single molecules/atomic-ions sensor, refractive index (RI) sensor, temperature sensor and humidity sensor.

1. Bio/chemical sensor

When a molecule binds onto a WGM resonator surface, the resonance frequencies of the optical modes will be shifted since the resonator's evanescent field is required to polarize the molecule[41]. Based on this principle, Su et al. developed a single-molecule sensor called frequency locked optical whispering evanescent resonator that can be used to detect a wide range of nanoscale objects with radii from 100 to 2.5 nm, including exosomes, ribosomes, mouse immunoglobulin G and human interleukin-2[41].

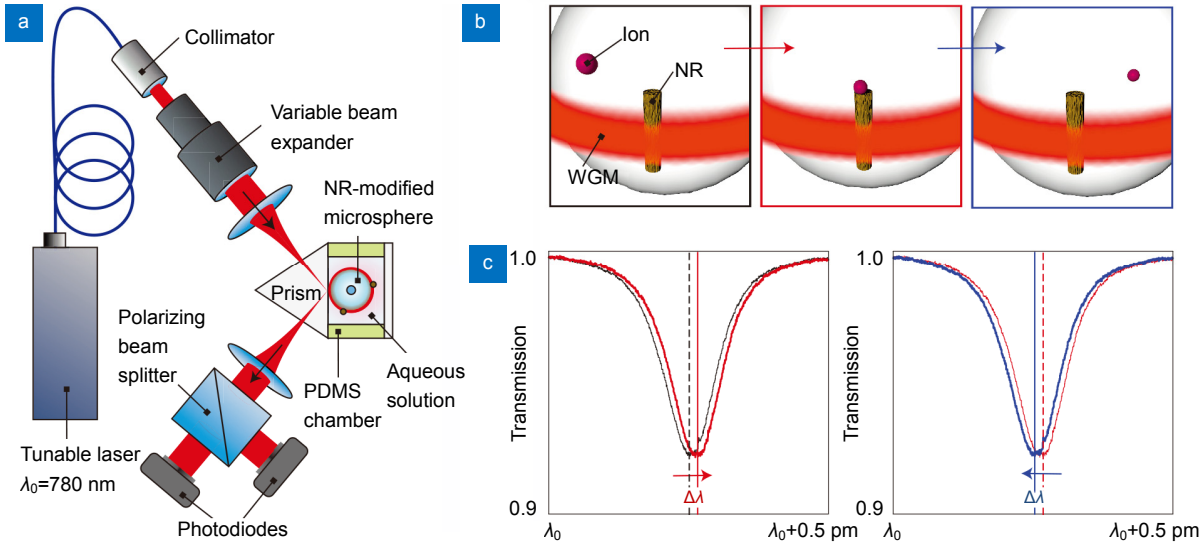

Fig. 3 | (**a**) Layout of the WGM sensing set-up. (**b**), (**c**) Transient interactions of single zinc or mercury ions with the NRs with the corresponding spectrum shifts. Figure reproduced from ref.[5], Springer Nature.

Besides detecting the nanoscale objects directly, WGM resonators can be applied to sensing a specific analyte by surface functionalization approaches. For example, Ghali et al. developed a biosensor by functionalizing the WGM microdisk with LysK for real-time detecting of Staphylococcus aureus, and the limit of detection is 5 pg/mL[42].

Swaim et al. built a theoretical model, in which WGM resonance frequency shifts can be enhanced through the combination of a microtoroid and a single Au nanorod, using the boundary element method in 2011[43]. After that, the sensing applications based on the combination between Au nanorod and microcavities have been widely studied. Recently, Baaske and Vollmer built a system utilizing a WGM sensing method to detect single atomic ions in an aqueous medium[5]. Gold nanorods (NRs) were bound onto the surface of a silica microsphere for exciting the NR's LSPR and generating local intensity hot spots at the tips of the NRs, and the hot spots can increase the resonance wavelength shift when single atomic ions interacted with plasmonic NRs, as shown in Fig. 3. In this work, the ion-NR interaction under different solution's ionic strength of both zinc and mercury ions was studied and a clear distinction of their behaviors was found.

Besides detecting the resonance wavelength shifts, there are also some intensity based WGM sensors. For instance, Heylman et al. demonstrated a single-particle photothermal absorption spectrometer by measuring the shift of the WGM energy[44]. This spectrometer applies on-chip optical WGM microtoroids as ultrasensitive thermmeters and is a convergence of narrow Fano resonances and WGMs, which makes it possess ultrahigh sensitivity up to sub-100 Hz resonance shift.

2. RI sensor

The resonant wavelengths of a microresonator have direct relationships with the RI difference between a microcavity and the surrounding medium. Therefore, microresonators with high Q factor can be applied as highly sensitive RI sensors, and these microresonators can be classified into passive microresonators and active microresonators. Compared with the RI sensors with passive microresonators[45,46], for example, Zhu et al. developed a RI detector utilizing liquid core optical ring resonators (LCORRs), and the sensitivity is 20 nm/RIU (refractive index units)[47], recently applying active microresonators to build RI sensors has been receiving more attention, since they can achieve the practical advantages of free space interrogation. By applying a high RI glue onto half of an active microsphere, Kang et al. demonstrated a RI sensor based on mode-splitting by the free space excitation[48]. This method is able to discriminate surrounding RI changes and temperature changes. Wan et al. developed a robust RI sensor using the dye-doped polymer microring laser based on the free-space optics measurement setup, which possessed the sensitivity of 75 nm/RIU[49]. Krämmer et al. utilized free-space optics to demonstrate that the RI sensitivity can be improved from 60 nm/RIU to 150 nm/RIU by decreasing the thickness of a dye-doped polymeric microdisk from 0.9 μm to 0.21 μm[50]. Ren et al. proposed a coupled liquid-core laser by the parallel placing of two thin-wall silica capillaries as shown in Fig. 4[51]. One of the

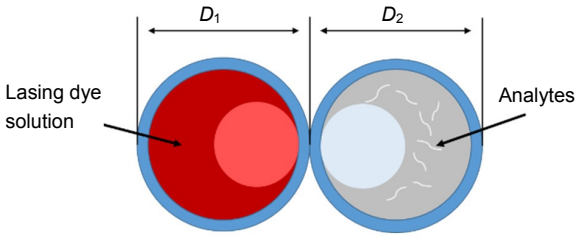

Fig. 4 | The illustration of the coupled liquid-core laser.

capillaries was filled with a dye solution, and the other one was injected with a sample. The sensitivity was up to 3874 nm/RIU by taking advantage of the Vernier effect.

3. Temperature sensor

Temperature variation can lead to the shift of resonant wavelengths of a microresonator, because it will induce a change of the microcavity refractive index and the microcavity size that are determined by the thermal optic coefficient and the thermal expansion coefficient of the microcavity. Hence, many temperature sensors based on WGM microresonators of different geometries and different materials were developed. The geometries included microspheres, microrings and microbubbles, and the materials included polymethyl methacrylate (PMMA), cholesteric liquid crystal (CLC), doped silicate glass, and doped oil. The sensitivities of these temperature sensors are shown in Table 1.

Table 1 | Sensitivities of temperature sensors based on WGM microresonator.

Microresonator	Sensitivity(nm/℃)
PMMA microbubble[38]	0.039
U-shaped optical fiber[52]	0.624
Doped polystyrene microparticle[53]	0.122
Silicon microring[54]	0.11
Dye-doped CLC microdroplet[55]	0.96
Holmium doped microsphere[56]	0.01
Doped oil mirodroplet[57]	0.377

4. Humidity sensor

Since the RI and size of some materials will vary when they absorb water vapor, the WGM microresonators consisting of these materials can be applied as humidity sensors. For example, Eryürek et al. presented an optical humidity sensor based on an on-chip SU-8 polymer microdisk, and demonstrated that the RI change of the microdisk was dominant when SU-8 interacted with water vapor[58]. Since SU-8 has the strong ability of interaction with water vapor, this sensor has a high sensitivity of 108 pm/% RH in the 0–1% RH range. Labrador-Páez et al. demonstrated a WGM microdroplet resonator that is made out of a 160 μm droplet of glycerol and rhodamine 6G adhered at the tip of an optical fiber[59]. Huang et al. developed an active microdisk of dye-doped PEG-DA hydrogel as a humidity sensor with a sensitivity of 43.11 pm/% RH[60]. The operating mechanism is that the size of the microdisk will homogenously be modified when the surrounding relative humidity changes, resulting in a linear shift of WGM lasing peaks.

Microlasers

Since Garrett et al. demonstrated the first WGM lasers in 1961[2], WGM microresonators have been widely used in the field of microlasers because of the high Q factor and the small mode volumes[8,25,53,61–64]. Due to these advantages, microlasers based on WGM microresonators can obtain an ultralow lasing threshold. The pump threshold is defined by the minimum pump power that is able to make cavity gain equal to loss in one round-trip. Moreover, microlasers based on WGM microresonators can naturally achieve very narrow linewidth due to the ultrahigh Q factor.

In 2017, Lim et al. fabricated a stabilized MgF_2 resonator laser with a 32 Hz Allan deviation and a sub-25 Hz linewidth by compensating the intrinsic thermal expansion of the WGM resonator[65]. Coating an active material onto a microresonator is another approach to fabricate the WGM microlaser. Fernandez-Bravo et al. developed a continuous-wave (CW) upconverting nanoparticle (UCNP) laser with a threshold of 14 kW/cm^2 by coating Tm^{3+}-doped energy-looping nanoparticles (ELNPs) onto a polystyrene microsphere with a diameter of 5 μm, as shown in Fig. 5[66]. This CW laser can work more than 5 hours at blue and near-infrared wavelengths.

Although light pumping is dominant in the field of WGM microlasers, electric current also can be applied as a pump source for a WGM microlaser. Moiseev et al. demonstrated a semiconductor microdisk laser that applied InGaAs quantum well-dots as an active area by photolithography and dry etching[67]. The pump threshold current density of this laser is 710 A/cm^2 for the microdisk of diameter of 31 μm, and around 70% of total absolute power (18.5 mW) is concentrated within the lasing modes.

As mentioned in Section 2, the WGM resonance wave-

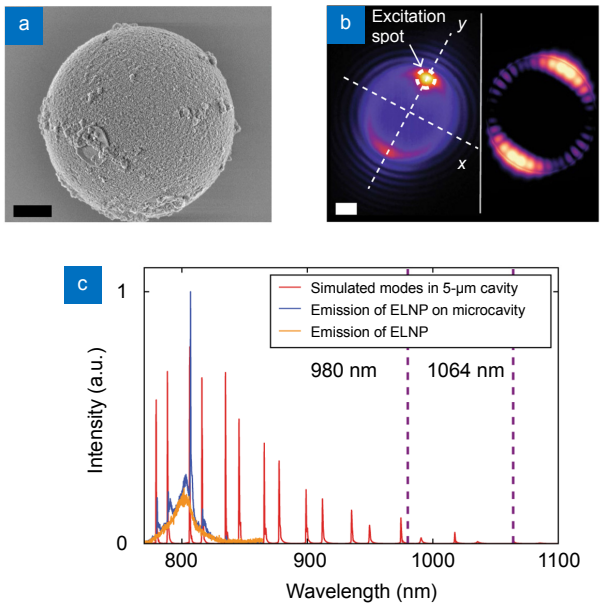

Fig. 5 | (**a**) Scanning electron micrograph of a polystyrene bead coated with ELNPs. (**b**) Left: wide-field image of a lasing microsphere. Right: simulated field distributions in the *x*–*y* plane. (**c**) Simulated NIR spectra of WGMs supported by a 5-μm polystyrene microsphere. Figure reproduced from ref.[66], Springer Nature.

length is closely related to microresonactor size, RI difference and so on. Hence, a tunable laser based on WGM resonance is feasible through cavity size modification. Zhu et al. developed an all-optical tunable microlaser based on an erbium-doped hybrid microbottle with a high Q factor of 5.2×10^7 and a low lasing threshold of 1.65 mW, as shown in Fig. 6[68]. This hybrid microbottle was generally fabricated as follows: first, attaching Er^{3+} ion solution onto the SMF surface; then, applying a CO_2 laser to process the SMF into a microbottle shape with a spherical end; finally, coating with iron oxide nanoparticles that can convert control light energy into thermal energy on the spherical end for tuning the lasing wavelength.

Besides these microlasers based on solid microcavities, Kiraz et al. demonstrated two types of optofluidic microlasers by combining aqueous quantum dots (QDs) and high Q factor optofluidic ring resonator (OFRR), as shown in Fig. 7[8]. One was achieved by filling 2 μM QDs with a bulk buffer solution into the OFRR cavity. The pump threshold of this microlaser could be down to 0.1 $\mu J/mm^2$. The other one was constructed by fixing a single layer of QDs onto the interface between the buffer solution and the OFRR inner wall. The surface density was from $3\times10^9\,cm^{-2}$ to $3\times10^{10}\,cm^{-2}$. In both cases, the laser emission persisted 5–10 min under uninterrupted pulsed excitation, which was a significant improvement compared with organic-dye-based lasers.

Since most WGM microcavities are circularly symmetric, the lasing emission is usually isotropic accordingly. In order to satisfy the requirement of unidirectional laser emission desired in many applications, some specially-designed microcavities have been proposed[61,69]. Zhan et al. fabricated a 3D polymer microlaser consisting of a stacked circular ring and a spiral ring on a narrow bandpass filter substrate by the femtosecond laser processing method[70]. The characteristic of this microlaser includes the low threshold of 60 $\mu J/cm^2$ and the unidirectional and single mode laser output. By comparing a series of different structures, they found that the circular ring is treated as an oscillator to generate the low-threshold WGMs lasing emissions, and the spiral ring serves as a mode filter and output port.

In addition, WGM microresonators also can be used to stabilize the laser and make it obtain a very narrow linewidth through their ultrahigh Q factors. A dual-microcavity laser was demonstrated by Loh et al., in 2015[7]. One on-chip silica microresonator was applied to generate tunable 1550 nm laser through stimulated Brillouin scattering (SBS) and another microresonator was used to stabilize the laser frequency, as shown in Fig. 8. The laser linewidth was approximately 87 Hz. The fractional frequency noise of this configuration was also reduced to $7.8\times10^{-14}\ Hz^{-1/2}$ when the offset was 10 Hz, which was a remarkable noise performance for a microresonator laser.

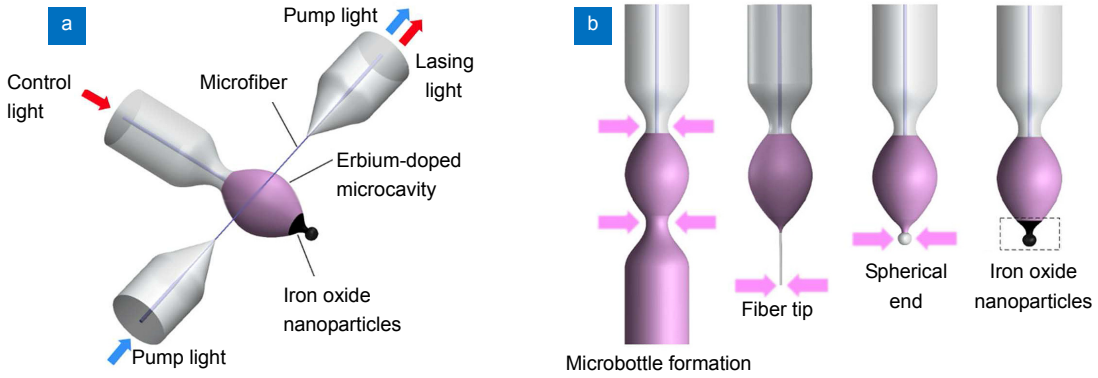

Fig. 6 | (**a**) Schematic of an all-optical tunable microlaser. (**b**) Fabrication process of the erbium-doped hybrid microbottle cavity coated with iron oxide nanoparticles. Figure reproduced from ref.[68], American Chemical Society.

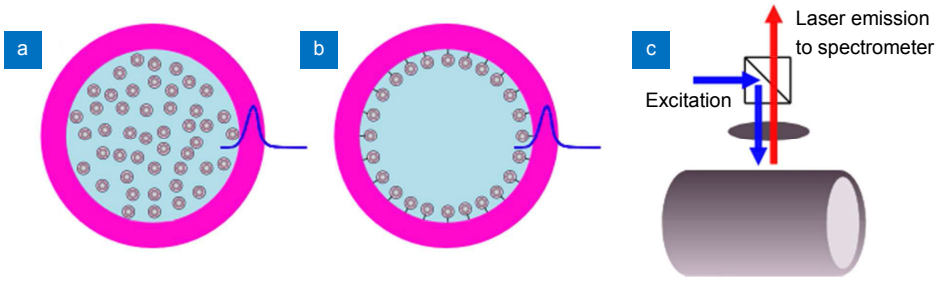

Fig. 7 | Illustrations of aqueous QDs (**a**) in solution inside an OFRR and (**b**) immobilized as a single layer on the inner surface of an OFRR. (**c**) Illustration of the experimental setup using confocal geometry. Figure reproduced from ref.[8], American Chemical Society.

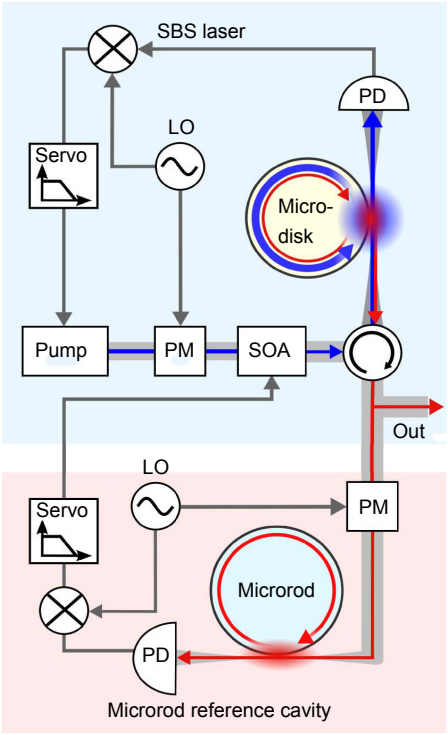

Fig. 8 | Diagram and operation of the dual-microcavity narrow-linewidth laser. Figure reproduced with permission from ref.[7], The Optical Society.

Conclusions and future prospects

In this paper, we have reviewed the key parameters and coupling conditions of WGM microresonators, geometries of WGM optical microcavities, and various applications in sensors and microlasers. Since the high Q factor can be easily obtained for WGM microresonators and the evanescent field exists around the surface of WGM microcavities, WGM resonance is extremely sensitive to the environment. This property gives the microresonators excellent behaviors even in detection of single atomic ions. On the other hand, microlasers based on WGM microresonators can achieve ultralow pump threshold and very narrow linewidth due to the ultrahigh Q factor and ultrasmall mode volume. These features are highly desired for mass production and future commercialization of the microlaser devices.

Although there are many significant research achievements of WGM in photonics[10,11,71–75], most of them are realized only in the laboratory with setups that require very careful alignment and positioning. For instance, sub-micrometer scale precision positioning is required to achieve effective coupling, as any variation in the distance between the microcavity and the coupler will result in a change of coupling efficiency and a change of the resonator performance. Furthermore, the coupler, such as a tapered fiber, with the diameter less than 2 μm, is fragile and is easily deteriorated by external air flow or dust. Hence, in our opinion, developing efficient, robust coupling methods and package approaches are crucial for practical applications of WGM microresonators in the future.

As mentioned in the Microlasers Section, since most WGM microcavities are circularly symmetric, the lasing emission is usually isotropic accordingly, but the requirement of unidirectional laser emission is highly desired in many applications. Although some specially-designed microcavities based on different unidirectional emission approaches such as scatter-induced unidirectional emission, chaos-induced unidirectional emission and grating-induced vertical emission, have been proposed[61,70,76] (for example Kim et al. proposed the design of the deformed microresonators for emission directionality by tailoring WGM properties[69]), the performance of unidirectional emission is required to be improved with respect to traditional laser performance.

Tunable lasing is an important branch in the field of lasers. Although some tunable microlasers based on WGM microresonators have been demonstrated, realizing the large tunable range and long lifetime are still challenging.

References

1. Rayleigh L. CXII. The problem of the whispering gallery. *Philos Mag* **20**, 1001–1004 (1910).
2. Garrett C G B, Kaiser W, Bond W L. Stimulated emission into optical whispering modes of spheres. *Phys Rev* **124**, 1807–1809 (1961).
3. Humar M, Yun S H. Whispering-gallery-mode emission from biological luminescent protein microcavity assemblies. *Optica* **4**, 222–228 (2017).
4. Zhu J G, Ozdemir S K, Xiao Y F, Li L, He L *et al*. On-chip single nanoparticle detection and sizing by mode splitting in an ultra-high-Q microresonator. *Nat Photonics* **4**, 46–49 (2010).
5. Baaske M D, Vollmer F. Optical observation of single atomic ions interacting with plasmonic nanorods in aqueous solution. *Nat Photonics* **10**, 733–739 (2016).
6. Matsko A B, Ilchenko V S. Optical resonators with whispering-gallery modes - Part I: Basics. *IEEE J Sel Top Quantum Electron* **12**, 3–14 (2006).
7. Loh W, Green A A S, Baynes F N, Cole D C, Quinlan F J *et al*. Dual-microcavity narrow-linewidth Brillouin laser. *Optica* **2**, 225–232 (2015).
8. Kiraz A, Chen Q S, Fan X D. Optofluidic lasers with aqueous quantum dots. *ACS Photonics* **2**, 707–713 (2015).
9. Yang S C, Wang Y, Sun H D. Advances and prospects for whispering gallery mode microcavities. *Adv Opt Mater* **3**, 1136–1162 (2015).
10. He L, Özdemir Ş K, Yang L. Whispering gallery microcavity lasers. *Laser Photonics Rev* **7**, 60–82 (2013).
11. Foreman M R, Swaim J D, Vollmer F. Whispering gallery mode sensors. *Adv Opt Photonics* **7**, 168–240 (2015).
12. Righini G C, Dumeige Y, Féron P, Ferrari M, Nunzi Conti G *et al*. Whispering gallery mode microresonators: fundamentals and applications. *La Rivista del Nuovo Cimento* **34**, 435–488 (2011).
13. Gohring J T, Dale P S, Fan X D. Detection of HER2 breast cancer biomarker using the opto-fluidic ring resonator biosensor. *Sensors Actuators B Chem* **146**, 226–230 (2010).

14. Lam C C, Leung P T, Young K. Explicit asymptotic formulas for the positions, widths, and strengths of resonances in Mie scattering. *JOSA B* **9**, 1585–1592 (1992).
15. Tang S K Y, Derda R, Quan Q M, Lončar M, Whitesides G M. Continuously tunable microdroplet-laser in a microfluidic channel. *Opt Express* **19**, 2204–2215 (2011).
16. Savchenkov A A, Matsko A B, Ilchenko V S, Maleki L. Optical resonators with ten million finesse. *Opt Express* **15**, 6768–6773 (2007).
17. Gorodetsky M L, Savchenkov A A, Ilchenko V S. Ultimate Q of optical microsphere resonators. *Opt Lett* **21**, 453–455 (1996).
18. Ta V D. Flexible whispering gallery mode optical microcavities for lasers and sensors (Nanyang Technological University, Singapore, 2014).
19. Vollmer F, Braun D, Libchaber A, Khoshsima M, Teraoka I *et al*. Protein detection by optical shift of a resonant microcavity. *Appl Phys Lett* **80**, 4057–4059 (2002).
20. Baaske M D, Foreman M R, Vollmer F. Single-molecule nucleic acid interactions monitored on a label-free microcavity biosensor platform. *Nat Nanotechnol* **9**, 933–939 (2014).
21. Chao C Y, Guo L J. Biochemical sensors based on polymer microrings with sharp asymmetrical resonance. *Appl Phys Lett* **83**, 1527–1529 (2003).
22. McCall S L, Levi A F J, Slusher R E, Pearton S J, Logan R A. Whispering-gallery mode microdisk lasers. *Appl Phys Lett* **60**, 289–291 (1992).
23. Sumetsky M, Dulashko Y, Windeler R S. Super free spectral range tunable optical microbubble resonator. *Opt Lett* **35**, 1866–1868 (2010).
24. Lee W, Sun Y Z, Li H, Reddy K, Sumetsky M *et al*. A quasi-droplet optofluidic ring resonator laser using a micro-bubble. *Appl Phys Lett* **99**, 091102 (2011).
25. Wang Y, Ta V D, Leck K S, Tan B H I, Wang Z *et al*. Robust whispering-gallery-mode microbubble lasers from colloidal quantum dots. *Nano Lett* **17**, 2640–2646 (2017).
26. François A, Riesen N, Gardner K, Monro T M, Meldrum A. Lasing of whispering gallery modes in optofluidic microcapillaries. *Opt Express* **24**, 12466 (2016).
27. White I M, Oveys H, Fan X D. Liquid-core optical ring-resonator sensors. *Opt Lett* **31**, 1319–1321 (2006).
28. Sarid D. High efficiency input-output prism waveguide coupler: an analysis. *Appl Opt* 18, 2921–2926 (1979).
29. Schiller S, Byer R L. High-resolution spectroscopy of whispering gallery modes in large dielectric spheres. *Opt Lett* **16**, 1138–1140 (1991).
30. Gorodetsky M L, Ilchenko V S. Optical microsphere resonators: optimal coupling to high-Q whispering-gallery modes. *JOSA B* **16**, 147–154 (1999).
31. Ilchenko V S, Yao X S, Maleki L. Pigtailing the high-Q microsphere cavity: a simple fiber coupler for optical whispering-gallery modes. *Opt Lett* **24**, 723–725 (1999).
32. Knight J C, Cheung G, Jacques F, Birks T A. Phase-matched excitation of whispering-gallery-mode resonances by a fiber taper. *Opt Lett* **22**, 1129–1131 (1997).
33. Dumeige Y, Trebaol S, Ghişa L, Nguyên T K N, Tavernier H *et al*. Determination of coupling regime of high-Q amplifiers resonators and optical gain of highly selective amplifiers. *JOSA B* **25**, 2073–2080 (2008).
34. Duan Z H, Wang Y J, Li G, Wang S, Yi N B *et al*. Chip-scale fabrication of uniform lead halide perovskites microlaser array and photodetector array. *Laser Photonics Rev* **12**, 1700234 (2018).
35. Huang S H, Sheth S, Jain E, Jiang X F, Zustiak S P *et al*. Whispering gallery mode resonator sensor for in situ measurements of hydrogel gelation. *Opt Express* **26**, 51–62 (2018).
36. Ward J M, Yang Y, Chormaic S N. Highly sensitive temperature measurements with liquid-core microbubble resonators. *IEEE Photonic Technol Lett* **25**, 2350–2353 (2013).
37. Ward J M, Yang Y, Chormaic S N. Glass-on-glass fabrication of bottle-shaped tunable microlasers and their applications. *Sci Rep* **6**, 25152 (2016).
38. He C H, Sun H J, Mo J, Yang C, Feng G Y *et al*. Temperature sensor based on high-Q polymethylmethacrylate optical microbubble. *Laser Phys*, **28**, 076202 (2018).
39. Yang Y, Lei F C, Kasumie S, Xu L H, Ward J M *et al*. Tunable erbium-doped microbubble laser fabricated by sol-gel coating. *Opt Express*, **25**, 1308–1313 (2017).
40. Han K, Kim J, Bahl G. High-throughput sensing of freely flowing particles with optomechanofluidics. *Optica* **3**, 585–591 (2016).
41. Su J, Goldberg A F, Stoltz B M. Label-free detection of single nanoparticles and biological molecules using microtoroid optical resonators. *Light Sci Appl* **5**, e16001 (2016).
42. Ghali H, Chibli H, Nadeau J L, Bianucci P, Peter Y A. Real-time detection of Staphylococcus aureus using Whispering Gallery Mode optical microdisks. *Biosensors* **6**, 20 (2016).
43. Swaim J D, Knittel J, Bowen W P. Detection limits in whispering gallery biosensors with plasmonic enhancement. *Appl Phys Lett* **99**, 243109 (2011).
44. Heylman K D, Thakkar N, Horak E H, Quillin S C, Cherqui C *et al*. Optical microresonators as single-particle absorption spectrometers. *Nat Photonics* **10**, 788–795 (2016).
45. Hanumegowda N M, Stica C J, Patel B C, White I, Fan X D. Refractometric sensors based on microsphere resonators. *Appl Phys Lett* **87**, 201107 (2005).
46. Ta V D, Chen R, Sun H D. Coupled polymer microfiber lasers for single mode operation and enhanced refractive index sensing. *Adv Opt Mater* **2**, 220–225 (2014).
47. Zhu H Y, White I M, Suter J D, Zourob M, Fan X D. Integrated refractive index optical ring resonator detector for capillary electrophoresis. *Anal Chem* **79**, 930–937 (2007).
48. Kang Y Q, François A, Riesen N, Monro T M. Mode-splitting for refractive index sensing in fluorescent whispering gallery mode microspheres with broken symmetry. *Sensors* **18**, 2987 (2018).
49. Wan L, Chandrahalim H, Zhou J, Li Z H, Chen C *et al*. Demonstration of versatile whispering-gallery micro-lasers for remote refractive index sensing. *Opt Express* **26**, 5800–5809 (2018).
50. Krämmer S, Rastjoo S, Siegle T, Wondimu S F, Klusmann C *et al*. Size-optimized polymeric whispering gallery mode lasers with enhanced sensing performance. *Opt Express* **25**, 7884–7894 (2017).
51. Ren L Q, Zhang X W, Guo X X, Wang H T, Wu X. High-sensitivity optofluidic sensor based on coupled liquid-core laser. *IEEE Photonics Technol Lett* **29**, 639–642 (2017).
52. Wu C W, Liu K C, Chiang C C. A novel U-shaped and microchanneled optical fiber temperature sensor fabricated by LIGA-like process. *IEEE Sensors J* **17**, 5444–5449 (2017).
53. Zeltner R, Pennetta R, Xie S R, Russell P S J. Flying particle microlaser and temperature sensor in hollow-core photonic crystal fiber. *Opt Lett* **43**, 1479–1482 (2018).
54. Nawrocka M S, Liu T, Wang X, Panepucci R R. Tunable silicon microring resonator with wide free spectral range. *Appl Phys Lett* **89**, 071110 (2006).

55. Zhao L Y, Wang Y, Yuan Y G, Liu Y J, Liu S Q *et al*. Whispering gallery mode laser based on cholesteric liquid crystal microdroplets as temperature sensor. *Opt Commun* **402**, 181–185 (2017).
56. de Sousa-Vieira L, Ríos S, Martín I R, García-Rodríguez L, Sigaev V N *et al*. Whispering gallery modes in a holmium doped glass microsphere: Temperature sensor in the second biological window. *Opt Mater* **83**, 207–211 (2018).
57. Liu Z H, Liu L, Zhu Z D, Zhang Y, Wei Y *et al*. Whispering gallery mode temperature sensor of liquid microresonastor. *Opt Lett* **41**, 4649–4652 (2016).
58. Eryürek M, Tasdemir Z, Karadag Y, Anand S, Kilinc N *et al*. Integrated humidity sensor based on SU-8 polymer microdisk microresonator. *Sensors Actuators B Chem* **242**, 1115–1120 (2017).
59. Labrador-Páez L, Soler-Carracedo K, Hernández-Rodríguez M, Martín I R, Carmon T *et al*. Liquid whispering-gallery-mode resonator as a humidity sensor. *Opt Express* **25**, 1165–1172 (2017).
60. Huang Q L, Xu H L, Li M T, Hou Z S, Lv C *et al*. Stretchable PEG-DA hydrogel-based whispering-gallery-mode microlaser with humidity responsiveness. *J Light Technol* **36**, 819–824 (2018).
61. Jiang X F, Xiao Y F, Zou C L, He L, Dong C H *et al*. Highly unidirectional emission and ultralow-threshold lasing from on-chip ultrahigh-Q microcavities. *Adv Mater* **24**, OP260–OP264 (2012).
62. Munnelly P, Lingnau B, Karow M M, Heindel T, Kamp M *et al*. On-chip optoelectronic feedback in a micropillar laser-detector assembly. *Optica* **4**, 303–306 (2017).
63. Wang Y Y, Xu C X, Jiang M M, Li J T, Dai J *et al*. Lasing mode regulation and single-mode realization in ZnO whispering gallery microcavities by the Vernier effect. *Nanoscale* **8**, 16631–16639 (2016).
64. Chandrahalim H, Chen Q S, Said A A, Dugan M, Fan X D. Monolithic optofluidic ring resonator lasers created by femtosecond laser nanofabrication. *Lab Chip* **15**, 2335–2340 (2015).
65. Lim J, Savchenkov A A, Dale E, Liang W, Eliyahu D *et al*. Chasing the thermodynamical noise limit in whispering-gallery-mode resonators for ultrastable laser frequency stabilization. *Nat Commun* **8**, 8 (2017).
66. Fernandez-Bravo A, Yao K Y, Barnard E S, Borys N J, Levy E S *et al*. Continuous-wave upconverting nanoparticle microlasers. *Nat Nanotechnol* **13**, 572–577 (2018).
67. Moiseev E, Kryzhanovskaya N, Maximov M, Zubov F, Nadtochiy A *et al*. Highly efficient injection microdisk lasers based on quantum well-dots. *Opt Lett* **43**, 4554–4557 (2018).
68. Zhu S, Shi L, Xiao B W, Zhang X L, Fan X D. All-optical tunable microlaser based on an ultrahigh-Q erbium-doped hybrid microbottle cavity. *ACS Photonics* **5**, 3794–3800 (2018).
69. Kim Y, Lee S Y, Ryu J W, Kim I, Han J H *et al*. Designing whispering gallery modes via transformation optics. *Nat Photonics* **10**, 647–652 (2016).
70. Zhan X P, Xu Y X, Xu H L, Huang Q L, Hou Z S *et al*. Toward on-chip unidirectional and single-mode polymer microlaser. *J Light Technol* **35**, 2331–2336 (2017).
71. Dong C H, Shen Z, Zou C L, Zhang Y L, Fu W *et al*. Brillouin-scattering-induced transparency and non-reciprocal light storage. *Nat Commun* **6**, 6193 (2015).
72. Förtsch M, Fürst J U, Wittmann C, Strekalov D, Aiello A *et al*. A versatile source of single photons for quantum information processing. *Nat Commun* **4**, 1818 (2013).
73. Pfeifle J, Coillet A, Henriet R, Saleh K, Schindler P *et al*. Optimally coherent Kerr combs generated with crystalline whispering gallery mode resonators for ultrahigh capacity fiber communications. *Phys Rev Lett* **114**, 093902 (2015).
74. Monifi F, Özdemir Ş K, Yang L. Tunable add-drop filter using an active whispering gallery mode microcavity. *Appl Phys Lett* **103**, 181103 (2013).
75. O'Shea D, Junge C, Pöllinger M, Vogler A, Rauschenbeutel A. All-optical switching and strong coupling using tunable whispering-gallery-mode microresonators. *Appl Phys B* **105**, 129–148 (2011).
76. Jiang X F, Zou C L, Wang L, Gong Q H, Xiao Y F. Whispering-gallery microcavities with unidirectional laser emission. *Laser Photonics Rev* **10**, 40–61 (2016).

Acknowledgements

This work is partially supported by National Natural Science Foundation of China (11774102), the Scientific Research Funds and Promotion Program for Young and Middle-aged Teacher in Science & Technology Research of Huaqiao University (ZQN-YX504, 17BS412), Open Fund of IPOC (BUPT), National Research Foundation Singapore (NRF) (NRF-CRP13-2014-05), European Union's Horizon 2020 Research and Innovation Programme under the Marie Sklodowska-Curie Grant Agreement (No. 798916) and Singapore Ministry of Education Academic Research Fund Tier 1 (RG89/16).

Competing interests

The authors declare no competing financial interests.